

Internal Report  
DESY F35D-95-15  
November 1995

# Perspectives of Tagged Structure Function Measurements in High Energy Lepton Scattering

by

N. A. Pavel



**DESY behält sich alle Rechte für den Fall der Schutzrechtserteilung und für die wirtschaftliche Verwertung der in diesem Bericht enthaltenen Informationen vor.**

**DESY reserves all rights for commercial use of information included in this report, especially in case of filing application for or grant of patents.**

**"Die Verantwortung für den Inhalt dieses  
Internen Berichtes liegt ausschließlich beim Verfasser"**

# Perspectives of Tagged Structure Function Measurements in High Energy Lepton Scattering

*Nikolaj A. Pavel*<sup>1</sup>

*II. Institut für Experimentalphysik  
Universität Hamburg, FRG*

## Abstract

Deep inelastic lepton scattering experiments have proven to be very successful in analysing the partonic substructure of nucleons. The structure functions extracted from the inclusive cross sections of lepton-nucleon (l-N) and lepton-nucleus (l-A) scattering carry the information about the parton distributions and correlation functions. For the search of subtle effects it is advantageous to select a subsample of events, for which the effect under investigation is expected to be enhanced, and to determine the cross section and related structure functions from the selected data.

So far the technique of 'tagged structure function' was primarily discussed in the context of the measurement of quark distributions at high  $x$  values in nucleons bound in nuclei. This technique should also be interesting for other aspects of the structure function analysis. Here some applications for ongoing or future electron scattering experiments will be discussed.

## 1 Introduction

For about 35 years the internal structure of nuclei and nucleons has been investigated in scattering experiments with high energy charged leptons. In deep inelastic lepton-nucleon scattering (DIS) the partonic substructure is studied. The object of quasi-elastic (QE) electron nucleus scattering ( $eA \rightarrow e'N(A-1)^*$ ) is the measurement of the momentum distribution and the correlation functions of the nucleons in a nucleus.

Since the contribution of the weak interaction is negligible in the kinematic range of the experiments discussed in this report, the incoming lepton couples to a current mediated by a photon, which probes the target. In contrast to photoproduction and hadron hadron (hh) or hadron nucleus (hA) reactions, multiple interaction of the incident particle inside the target nucleus or nucleon can be ignored. This property and the pointlike nature of leptons make electrons and muons ideal projectile particles for structure analyses.

The structure functions, which are extracted from the measured cross section of QE and DIS, contain the information about the substructure of the target. From their dynamical evolution information about the forces between the constituents can be deduced. However, if small effects or threshold effects in the structure function are investigated, it is often not sufficient to measure the global structure function. Instead it is better to select a subsample of events, for which the effect under study is expected

---

<sup>1</sup>invited talk at the 8-th Miniconference 'Correlation in Nuclei and Nucleons',  
Amsterdam, December 1993 (reprint of contribution to the Conference Proceedings)

to be more pronounced. This can e.g. be achieved by the observing final state particles in coincidence with the scattered lepton. In this report, structure functions, which are obtained from such "exclusive" subsamples, will be called 'tagged structure functions' (TSF).

The tagging strategy must be such that the events for effect under study are selected with high efficiency, while at the same time the large background from the untagged QE or deep inelastic events is suppressed.

Examples of tagged structure function (TSF) analyses are the evaluation of the gluon structure function from heavy flavour production in DIS or the extraction of the  $\pi$ -structure function from the cross section of the Drell-Yan process. In this report I will focus on some new applications which are proposed for ongoing and future  $e$ - $p$  scattering experiments.

In section 2 I start by discussing to which extent TSF can be used for the investigation of correlations between nucleons in nuclei and partons in bound nucleons. The search for 'hot spots' in DIS at very small values of the scaling variable  $x$  (Bjorken scaling variable) in DIS is studied in section 3. Section 4 is devoted to diffractive scattering with highly virtual photon and the possibility of obtaining information about the nature of the pomeron. The conclusion are presented in section 5.

## 2 Correlation of Nucleons and Partons in Nuclei

For a long time the determination of nucleon momentum distributions in nuclei was exclusively the domain of traditional nuclear physics and it was believed that nuclear effects could safely be ignored if the partonic substructure of nucleons is investigated at a high  $Q^2$  ( $Q^2 > 1 \text{ GeV}^2/c^2$ ), where  $Q^2$  is the negative square of the mass of the virtual boson exchanged between the lepton and the target.

The discovery of the EMC effect [2] has shown that the parton distributions in nucleons which are determined via the structure function  $F_2$  of nucleons bound in nuclei, are influenced by the surrounding nuclear matter. In fig. 2.1 the ratio of the deep inelastic structure function of bound and free nucleons,  $R_{EMC} := F_2^A/F_2^N$ , is plotted as a function of the Bjorken scaling variable  $x$ . The atomic mass number  $A$  is in the range of 60 and  $N$  stands for the free nucleon, averaged between proton and neutron ( $N = \frac{1}{2}(p + n)$ ). The structure function  $F_2^N$  has been obtained from scattering on deuterium, which is the smallest isoscalar target available. The ratio exhibits a significant and characteristic deviation from unity. For further discussion it is customary to subdivide the  $x$ -range in 5 zones (see fig. 2.1):

**zone 1:** There is a sizeable reduction of the cross section at small  $x$ . This can be explained in a consistent way by nuclear shadowing effects [4]. Because of the large energy ( $\nu$ ) of the virtual photon exchanged, the lifetime of a hadronic quantum fluctuation of the photon is Lorentz dilated in the rest frame of the nucleus. In deep inelastic scattering the probability for a quantum fluctuation of the virtual photon into a vector meson decreases towards higher  $Q^2$  like  $1/(Q^2 + m_{meson}^2)$ ; however this is partially compensated because of the high energy of the photons, so that nuclear

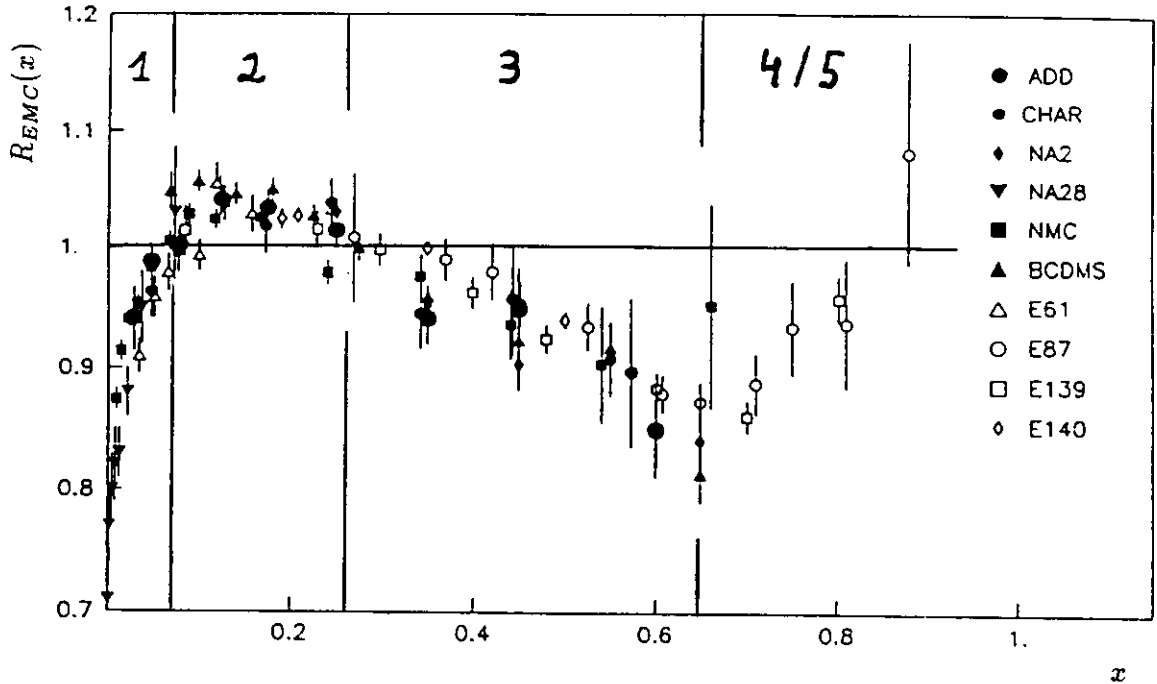


Fig. 2.1. Compilation of experimental results for  $R_{EMC} = F_2^A/F_2^N$  (EMC effect) [3] for  $A$  in the range of 60 ; zones 1-5 are defined in the text.

shadowing as observed for real photoproduction is possible also for virtual photons.

**zone 2:** The slight enhancement of  $R_{EMC}$  above unity ("antishadowing") is in most models attributed to the recombination of partons at lower  $x$  [5]. It is not yet clear whether this is the only possible explanation.

**zone 3:** There is a plethora of models based on very different ideas (see e.g. [6, 12]), which reproduce the behaviour of  $R_{EMC}$  in this range of  $x$ . In order to discriminate between the various ansatzes, one has not only to improve the precision of the existing measurements but in addition has to find new observables to test some of the specific hypotheses, like the idea of increased effective confinement radius for bound nucleons, the influence of nuclear binding forces or the contribution of virtual  $\pi$ ,  $\Delta$  or other nucleon resonances.

**zone 4:** Even before the discovery of the EMC effect differences between the structure function of free and bound nucleons had been observed in this range of  $x$ . They have been ascribed to the Fermi motion of the nucleons inside the nucleus ( see e.g. [7]). In addition to the range of  $x$  values below  $x = 1$  a measurement of the ratio  $R_{EMC}$  for  $x > 1$  looks particularly promising, since in this kinematic region the quantity  $R_{EMC}$  should be sensitive to the presence of multi-quark configurations with more than

three valence quarks. Multi-nucleon clusters have been studied extensively in nuclear physics and models based on such phenomena are successfully applied to describe the properties of nuclei. This suggests to look for correlations amongst partons across the classical nucleon boundaries.

## 2.1 Correlation of Nucleons in Nuclei

Correlations between nucleons (NN-correlations) are being investigated in many experiments of QE electron nucleus scattering and nucleon knock out reactions induced by hadrons or real photons. This type of reaction is discussed in detail in several other contributions to these proceedings [8]. Here I will briefly recall some facts and relations pertinent to the following discussion.

The cross section for QE electron nucleus scattering can be written as:

$$\sigma_{QE}(Q^2, \nu) = \sum_{n=1}^A \int dE_N d^3k_N S_N(\mathbf{k}_N, E_N) * \sigma_{eN} \delta(k_N - k'_N - q) \quad (2.1)$$

where  $k_N = (E_N, \mathbf{k}_N)$  and  $k'_N = (E'_N, \mathbf{k}'_N)$  are the four-momenta of the nucleon before and after scattering with the photon ( $\gamma^*$ ) with four momentum  $q = (\nu, \mathbf{q})$  in the N rest frame and  $Q^2 = -q^2$ .  $\sigma_{eN}$  is the cross section for elastic electron nucleon scattering. The spectral function  $S_N$  represents the combined probability to find in the nucleus a nucleon with momentum  $k_N$  and energy  $E_N$  or equivalently that the rest nucleus ( $A - 1$ ) is left with an intrinsic excitation energy  $E_{A-1}^*$ .

From  $S_N$  the nucleon momentum density function  $n(k_N)$  can be derived by:

$$n(k_N) = \int_{E_{min}}^{\infty} S_N(\mathbf{k}_N, E_N) dE_N \quad (2.2)$$

Introducing a nuclear structure function:

$$F(Q^2, y) = 2\pi \int_{E_{min}}^{\infty} dE_N \int_{k_{N,min}(q,y,E_N)} S_N(\mathbf{k}_N, E_N) dk_N \quad (2.3)$$

$\sigma_{QE}$  can be written in the plane wave impulse approximation (PWIA) in the factorizing ansatz:

$$\sigma_{QE} = F^{eep}(Q^2, y) * (Z * \sigma_{ep} + (A - Z) * \sigma_{en}) \frac{dy}{dk_N d \cos \alpha} \quad (2.4)$$

where  $\alpha$  is the angle between the exchanged photon and the scattered nucleon,  $Z$  is the charge of the nucleus and  $\sigma_{ep}, \sigma_{en}$  are the elastic  $e-p$  ( $e-n$ ) cross sections respectively.

The structure function  $F^{eep}$  scales approximately in the variable  $y$ , which represents the minimum momentum of the nucleon with minimal removal energy. The influence of final state interactions can be ignored when considering the asymptotic structure function  $\lim_{Q^2 \rightarrow \infty} F^{eep}(Q^2, y)$ . The residual scaling violation can be entirely ascribed to NN-correlations. Short range correlations of this type have been found to

be responsible for the large deviations of the measured  $n(k_N)$  from the prediction of the mean field approximation (see [9]).

NN-correlations can also be studied by extracting  $F(Q^2, y)$ , and hence  $n(k_N)$  from tagged events, where a second nucleon with momentum  $k_2$  is detected in coincidence (see fig. 2.2). Within the spectator mechanism [17, 10] the result can be interpreted as QE scattering on a nucleon which belongs to a correlated pair. In this model of "bound" pairs of nucleons there is a momentum transferred to the spectator nucleon leading to a recoiling nucleon.

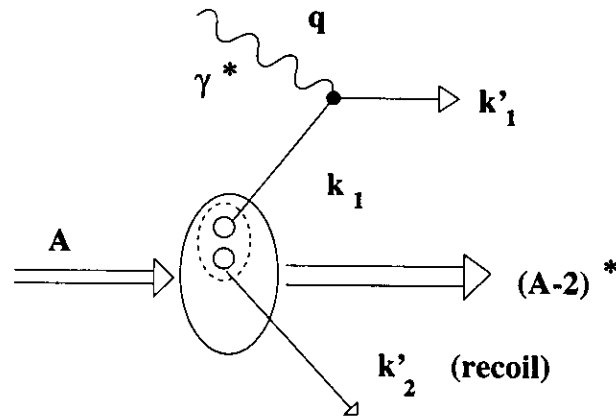


Fig. 2.2. Schematic diagram describing tagged quasi elastic electron nucleus (A) scattering.

The impulse spectrum ( $n(k_N)$ ) measured at different values of the recoil momentum  $k_2$  provides information about the frequency of correlated pairs and the strength of the binding of such pairs.

## 2.2 Tagging Structure Functions in Deep Inelastic Lepton Nucleus Scattering

In the zone 3 ( $0.25 < x < 0.65$ ), it is necessary to discriminate between many possible explanations proposed in various publications. Additional and new constraints from experimental data are required to find a unique solution. In this report I will discuss whether TSF measurement can contribute to the solution of the problem.

It is quite natural to search for relationships between the properties of the nucleus and the observed size of the nuclear effect on the parton distribution functions, i.e. in  $R_{EMC}$ . In fact, there is a large class of proposed explanations, which deal with conventional nuclear corrections.

The basis of these models is an ansatz for the structure function of the bound nucleon ( $F_2^A$ ), which is expressed as the convolution integral of two structure functions:

$$F_2^A(x) = \sum_{all\ const.} \int_x^{M_A/M_N} f_{C/A}(y_A) * F_{q/C}(x_A/y_A) dy_A \quad (2.5)$$

where  $f_{C/A}$  represents the probability to find a constituent  $C$  with the light cone momentum fraction  $y_A = P_C^+/P_A^+$  in the nucleus;  $P_C^+$  and  $P_A^+$  are the positive light cone momenta ( $P^+ = E + P_z$ ) of the constituent and the nucleus respectively. The constituent  $C$  is usually a nucleon but might also be a virtual exchange particle like a  $\pi$  or  $\Delta$  [11].  $F_{q/C}$  is the structure function  $F_2^N$  of the free nucleon. With  $x_A = p_{quark}^+/P_A^+$  the Bjorken scaling variable becomes  $x = x_A/y_A$ .

For a simplified Fermi gas model  $f_{C/A}$  would have the form:

$$f_{C/A} = A * \delta \left( y_A - \frac{1}{A} \left( 1 + \frac{B}{M_N} \right) \right) \quad (2.6)$$

$$\Rightarrow F_2^A(x) = F_2^N \left( x * \left( 1 - \frac{B}{2M_N\nu} \right) \right) \quad (2.7)$$

where  $B$  is the nuclear binding energy and  $\nu$  the virtual photon energy in the proton rest frame. Binding energy effects predict  $F_2^A(x)$  to be equal to  $F_2^N(x')$  at a value of  $x'$  which is slightly larger than  $x$  ( $x$ -rescaling), since  $B < 0$  by definition. Thus  $R_{EMC}$  should always be smaller than unity and the deviation should increase towards higher  $x$ .

Considering the underlying Fermi motion of the nucleons it is possible to reproduce the ratio  $R_{EMC}$  in the medium  $x$ -range reasonably well, provided one has chosen the proper value for the effective binding energy  $\langle \epsilon \rangle$  [12] (see fig. 2.3).  $\langle \epsilon \rangle$  and the average kinetic energy of the constituents ( $\langle T \rangle$ ) in turn depends on the impulse spectrum  $n(k_N)$  and the function  $f_{C/A}$  is related to the spectral function and so to  $n(k_N)$  by:

$$f_{C/A} = \int d^4 p_C S_N(P_C) y_A \delta \left( y_A - \frac{P_C q}{P_A q} \right) \quad (2.8)$$

As outlined in section 2.1 there is strong evidence from QE scattering experiments for the presence of NN-correlations with a binding potential higher than the average nuclear value. First calculations of  $R_{EMC}$ , in which short range correlations are considered, have been performed [13]. Up to now only the trend of the experimental data could be reproduced and more detailed information is needed.

It has been suggested [15, 17] to measure the ratio of the tagged structure function  $\bar{R}_{EMC}(x, k'_2)$  in deep inelastic scattering requiring a recoil nucleon with a four momentum  $k'_2$ . Applying the same arguments as in section 2.1, this nucleon is interpreted as the partner of a correlated NN-pair in the nucleus, which recoils when the other partner is hit by the virtual photon.

In fig. 2.4 the cross section at  $Q^2 = 10 \text{ GeV}^2/c^2$  and various values of  $x < 1$  is shown for two emission angles of the recoil proton, (a) for forward emission and (b) for backward emission. Here, the forward and backward hemisphere are defined as the region of  $\vartheta_2 > 90^\circ$  ( $\vartheta_2 < 90^\circ$  resp.), where  $\vartheta_2$  is the angle between the recoil nucleon and the virtual photon momentum. The cross section is plotted as a function of the kinetic energy of the recoil nucleon  $T_2 = (k'_2)^2/(2M_N)$ . The calculations are performed

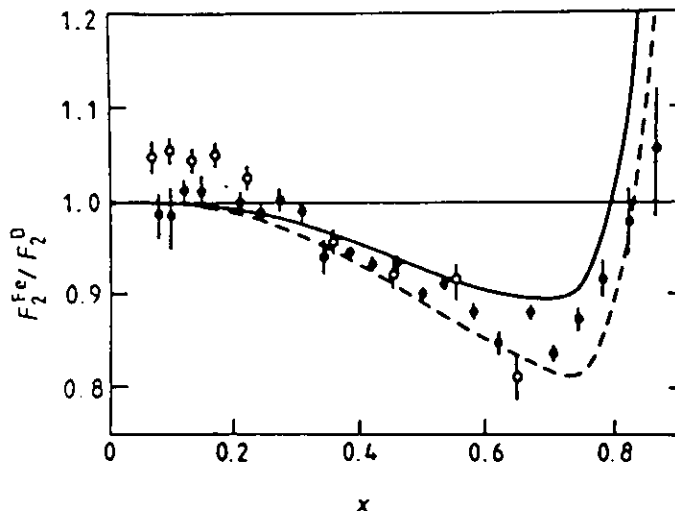


Fig. 2.3.  $R_{EMC}$  for iron over deuterium compared with model calculations for different binding energies  $\langle \epsilon \rangle$ :  $\langle \epsilon \rangle = -26 \text{ MeV}$  [13] (solid line) and  $\langle \epsilon \rangle = -39 \text{ MeV}$  [14] (dashed line).

using two different ansatzes for the spectral function of the NN-pair: (a) a simplified model, where the correlated pair is at rest in the nucleus [17], and (b) an extended NN-correlation model, which takes into account the motion of the center of mass of the NN-pair ( $k_{cm}$ ).

For forward emitted recoil nucleons the results are insensitive to the choice of the two-nucleon spectral function, in contrast to the backward emission region. This is so, since the condition  $z_1 = 2 - z_2 - k_{cm}^{\parallel}/M_N > x$  can be satisfied for forward emission at any value of  $k_2$  both with  $k_{cm} = 0$  and with  $k_{cm} \neq 0$ , whereas for nucleons emitted backwards  $k_{cm} \neq 0$  is required for  $k_2 > 0$ . The variables  $z_i = k_i^+ / M_N$ , ( $i = 1, 2$ ) define the scaled positive light cone momenta of the two nucleons of the NN-pair, as measured in the frame, where the momenta of the virtual photon and the nucleus are collinear. Thus, high momentum nucleons that recoil in the backward hemisphere signal short range correlations in the initial state.

The aim of the TSF analysis is the test of nuclear effects on the structure function of bound nucleons, which may manifest itself as  $x$ -rescaling of  $F_2^A$ . The double ratio:

$$R_{DBL}(x, x', k_2) = \left( \frac{\bar{F}_2^A(x, k_2)}{\bar{F}_2^A(x', k_2)} \right) / \left( \frac{F_2^N(x)}{F_2^N(x')} \right), \quad \text{with } F_2^N = \frac{1}{2}(F_2^p + F_2^n) \quad (2.9)$$

is significantly less dependent on the model used for the NN-spectral function. Thus this quantity, shown in fig. 2.5 for the forward and the backward emission of the recoil nucleon and various momenta  $k_2$ , is sensitive to possible changes in the structure function itself and can be used to look for nuclear effects.

Since for forward emission ( $z_2 < 1$ ) the ratio  $x/z_1$  is always smaller than  $x$  the double ratio is larger than unity and grows when demanding larger values for the

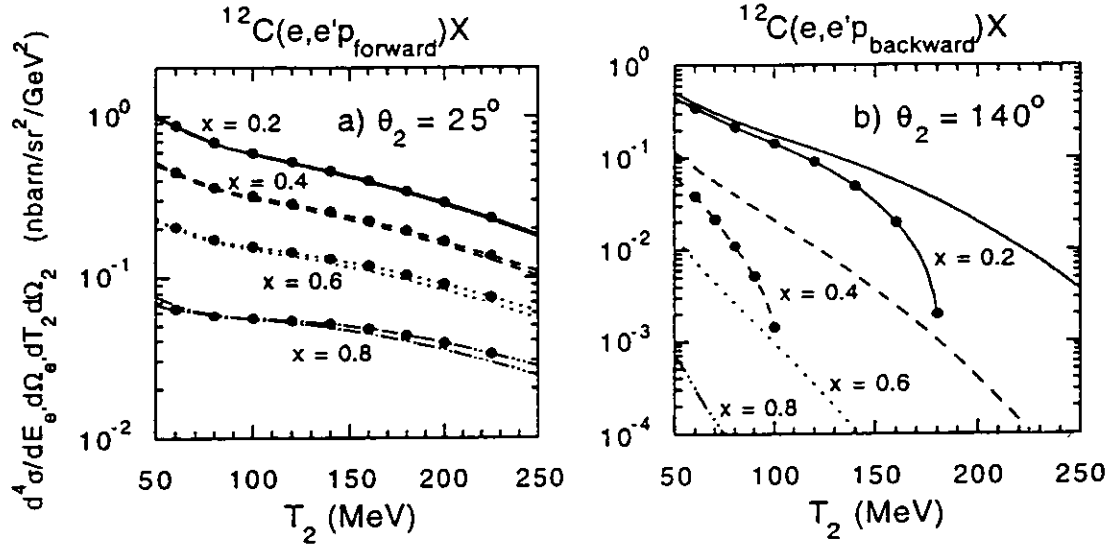


Fig. 2.4. Calculated cross section for tagged DIS events at  $Q^2 = 10 \text{ GeV}^2/c^2$  and various values of  $x$  for forward (a) and backward (b) emitted recoil nucleons [15] as function of the recoil nucleon energy  $T_2$ . Curves with (without) points show results with a simplified (extended) NN-correlation model (see text)

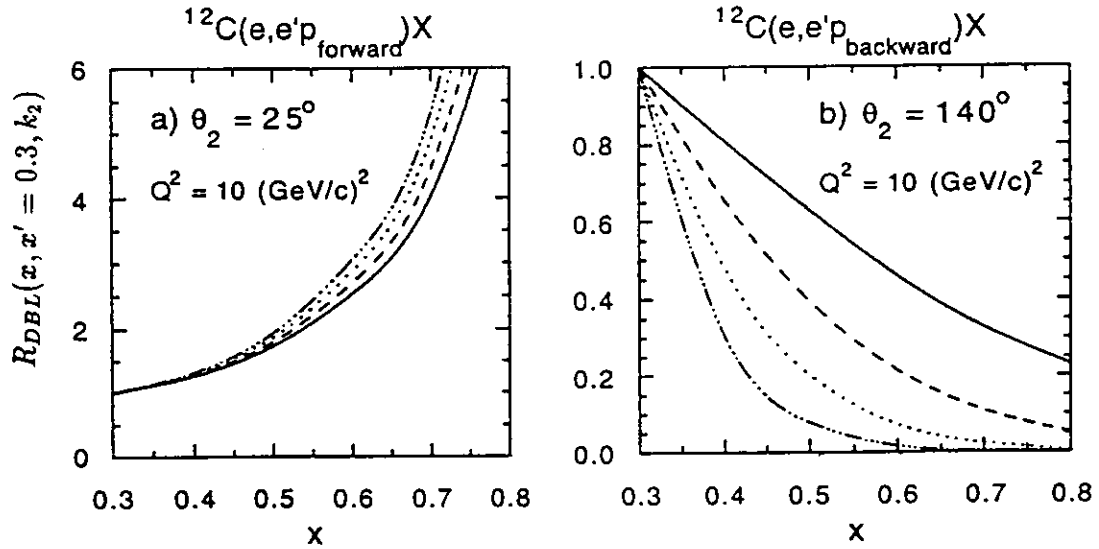


Fig. 2.5. The double ratio of tagged structure functions  $R_{DBL}$  (equ.2.9 for  $x' = 0.3$ ) calculated with the extended model for NN-correlation [15]. The solid, dashed, dotted and dashed-dotted lines are results for  $T_2 = 0.3, 0.4, 0.5, 0.6 \text{ GeV}/c$  respectively. The electron beam energy is  $E_{beam} = 30 \text{ GeV}$ .

momentum of the recoil nucleon. For nucleons emitted backward ( $z_2 > 1$ ) the inverse correlation is found since  $x/z_1 > x$ .

The kinematic region  $x > 1$  is obviously well suited for testing models which are based on multi-quark configurations. However the interpretation of TSF measurements will require a careful treatment of the NN-spectral function.

The identification and measurement of the recoil nucleon is a crucial point in any analysis of this type. Fig. 2.6 shows for the process  $ed \rightarrow e'p_{recoil}X$  the momentum of the recoil proton (line) and of the protons from the fragmentation process as function of the relative momentum of the proton before the hard scattering; the Fermi momentum  $k_F$  is equivalent to momentum  $k_2$  used in the above discussion. For a wide range of  $k_2$  the recoil proton is sufficiently well separated in the momentum space.

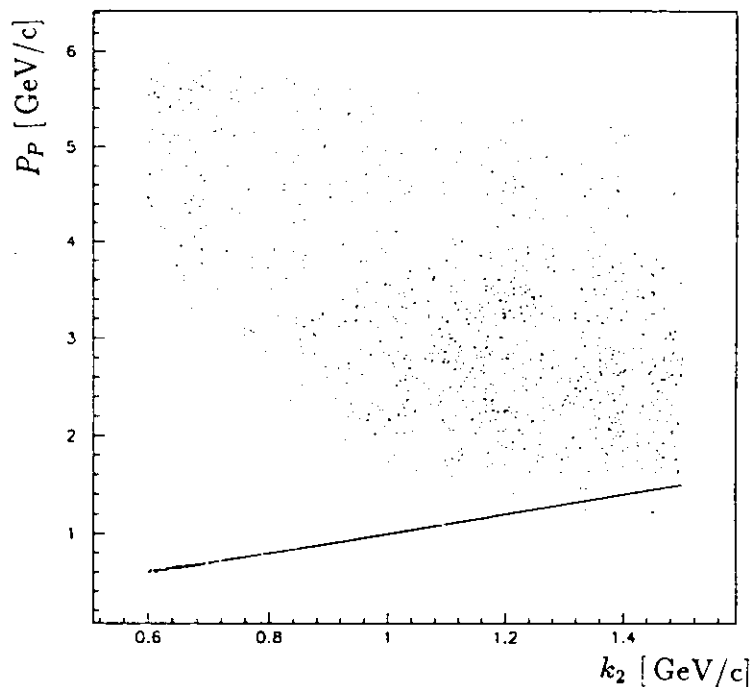


Fig. 2.6. Momenta of protons produced in the tagged DIS process [16] :  $ed \rightarrow e'X + p_{recoil}$  as a function of the momentum  $k_2$  of the proton before the hard scattering; the line in the lower part of the scatter plot represents the narrow band of the recoil proton momenta.

For more complex nuclei, however, the situation is more complicated due to protons emerging from the target fragmentation and the final state interaction of the slow recoil nucleons with the residual nucleus. The influence of both these effects has been estimated using a factorizing ansatz together with the diquark fragmentation function of [18] and the distorted wave impulse approximation [10]. For light nuclei ( $^{12}C$ ) it was found [15] that TSF with backward emitted nucleons are only little affected. For forward emission the expected corrections are still acceptable for  $0.3 < k_2 < 0.7$  GeV. For heavier targets the applicability of this kind of analysis has to be questioned because

of the large expected corrections.

An experiment of this kind requires a very high luminosity and a detector which can operate at high event rates. The identification of the recoil nucleon and the measurement of its energy with a precision better than the pion mass is a challenging task for experimental facilities of the next generation, which are now under discussion (e.g. [19]).

### 3 Parton Correlations in the Proton at small $x$

#### 3.1 Dynamical Evolution of Parton Distributions

At HERA the DIS cross section can be measured down to very small  $x$  ( $x \sim 10^{-4}$ ), at values of  $Q^2$  ( $Q^2 > 4 \text{ GeV}^2/c^2$ ) where the strong coupling constant  $\alpha_s$  is still small enough so that perturbative QCD can be applied.

At not too small values of  $x$  ( $x > 0.01$ ) the dynamical evolution of the structure function is described by the DGLAP integro differential equations in excellent agreement with the data [20]. The solution of these equations gives, loosely speaking, the probability to find a parton with a transverse size  $\sim 1/Q$  inside the proton at fixed  $x$ . As with increasing  $Q^2$  this probability decreases and also the transverse size shrinks, the proton is essentially "empty" at high  $Q^2$  and not too small  $x$ .

The opposite is true if  $x$  is decreased at fixed  $Q^2$ . For  $x < 0.01$  the structure function  $F_2$  is almost entirely given by the sea quark and the gluon density functions. The gluon density is expected to increase with decreasing  $x$  due to multiple gluon branching processes, which can be depicted in the form of ladder diagrams. At fixed  $Q^2$  the behaviour of the gluon density function  $xg(x, Q^2)$  is given by the solution of the BFKL equation (table 3.1). The integral kernel contains the splitting functions as well as lowest order virtual correction to the branching process. At high  $Q^2$  and low  $x$  the double leading log approximation (DLLA) is used.

In both evolution schemes, the DLLA and the BFKL evolution, the gluon density grows beyond any limit towards  $x \rightarrow 0$ . Since the transverse size of the partons is fixed by  $1/Q$  and since the partons are confined in the proton, there must be a critical value of  $x$  ( $x_{crit}$ ) below which recombination processes lead to a saturation of the parton density.

At even lower values of  $x$  the cross section becomes large and the high number of partons involved in the process does not allow the application of conventional methods of perturbative QCD, although  $\alpha_s$  remains small (Regge limit).

In the transition region between the Regge domain and the domain of steadily growing  $F_2$ , one considers two competing processes: the emission of gluons  $\propto g(x, Q^2)/(\pi R_{proton}^2)$  and the annihilation of gluons, that is proportional to a term  $[g(x, Q^2)]^2/(\pi R_{proton}^2)$ , which is not linear in  $\alpha_s$ . Gribov, Levin and Ryskin have added a non-linear term to the DGLAP and DLLA equations [21]:

$$\frac{\partial^2 xg(x, Q^2)}{\partial \ln \frac{1}{x} \partial \ln Q^2} = \alpha_s \frac{xg(x, Q^2)}{\pi R^2} - \frac{\alpha_s^2}{Q^2} * \frac{const}{R^2} [xg(x, Q^2)]^2 \quad (\text{modified DLLA}) \quad (3.1)$$

$$x \frac{\partial g(x, Q^2)}{\partial \ln Q^2} = K \otimes g(x, Q^2) - \frac{81\alpha_s^2}{16R^2 k_\perp^2} x^2 (g(x, Q^2))^2 \quad (GLR) \quad (3.2)$$

These negative colour screening corrections are proportional to  $1/R^2$ , where  $R$  is the effective confinement radius for the partons. Hence, if the partons are concentrated in spaces smaller than the proton, so called hot spots, the non-linear forces between the partons are stronger and they will be observable already at higher  $x$ .

range of validity	name	equation for gluon
$\alpha_s \ln Q^2 = \mathcal{O}(1)$ $\alpha_s \ln \frac{1}{x} \ll 1$	DGLAP	$\frac{\partial xg(x, Q^2)}{\partial \ln Q^2} = \frac{\alpha_s}{2\pi} [P_{gq} \otimes \sum_i q_i + P_{gg} \otimes g]$ $P_{gq}, P_{gg} = \text{splitting functions}$
$\alpha_s \ln Q^2 \ll 1$ $\alpha_s \ln \frac{1}{x} = \mathcal{O}(1)$	BFKL	$\frac{\partial xg(x, Q^2)}{\partial \ln \frac{1}{x}} = K \otimes g = \lambda * g(x, Q^2)$ $\Rightarrow xg(x, Q^2) \propto x^\lambda ; \lambda \sim (-0.5)$ $K = \text{integral kernel}$
$\alpha_s \ln Q^2 = \mathcal{O}(1)$ $\alpha_s \ln \frac{1}{x} = \mathcal{O}(1)$	DLLA	$\frac{\partial^2 xg(x, Q^2)}{\partial \ln Q^2 \partial \ln \frac{1}{x}} = \frac{3\alpha_s}{\pi} xg(x, Q^2)$ $\Rightarrow xg(x, Q^2) \propto \exp \left\{ \sqrt{2} \sqrt{\frac{3\alpha_s}{\pi}} \ln Q^2 \ln \frac{1}{x} \right\}$

Tab. 3.1. Overview over the evolution equations for the gluon density function in the kinematic range of  $x$  and  $Q^2$  accessible at HERA.

### 3.2 Search for Hot Spots in the Proton

One of the primary objectives at HERA is the study of a system of strongly interacting objects at high densities but relatively small strong coupling constant, where one expects a non-linear evolution pattern and the transition to the Regge domain.

The presence of the new parton interactions described by equ. 3.1, 3.2 would manifest itself in a suppression of the diffractive cross section. The deviation from the standard evolution pattern may still be very small in the range of  $x$  and  $Q^2$  accessible at HERA. But for a sample of events in which the interacting partons are confined to a volume smaller than the proton ( $R < R_{\text{proton}}$ ), the cross section is more sensitive to this new effect.

A method to tag such events has been proposed in [22]: One has to select DIS events with a jet in addition to the jet resulting from the struck quark ("current jet"). This extra jet is characterized by the momentum fraction  $x_{\text{jet}}$  and the transverse momentum  $\vec{k}_\perp^2$ , where  $\vec{k}_\perp^2$  has to be measured in a frame, in which the virtual photon and the incident proton are collinear. The variables  $x_{\text{jet}}$  and  $\vec{k}_\perp^2$  have to fulfill the

conditions:  $x_{jet} \gg x$  and  $\bar{k}_\perp^2 \sim Q^2$ . The first condition ensures that there is a large rapidity difference between the struck parton and the extra jet (see fig. 3.1). Therefore one can assume that the photon quark ( $\gamma^* - q$ ) vertex and the vertex of the gluon emission are connected by a gluon ladder. As result of the second tagging condition the extra jet has about the same transverse momentum as the struck parton. So, there will be not much evolution in  $Q^2$  between the photon and the jet vertex.

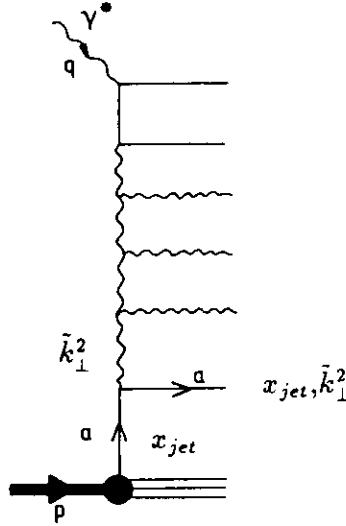


Fig. 3.1. Schematic diagram to illustrate the tagging conditions for the 'hot spot' search.

Thus the partons involved in the observed process must be concentrated in a space which has a transverse dimension  $R \sim \sqrt{\Delta \bar{k}_\perp^2} = \sqrt{Q^2 - \bar{k}_\perp^2}$ . The parton density in that volume which is  $\propto r_x = x_{jet}/x$ , should be of the order of  $10^2$  to justify the gluon ladder ansatz [23]. Fig. 3.2 shows the size of the colour screening correction (equ. 3.1,3.2) for different values of  $\Delta \bar{k}_\perp^2$  and  $r_x$ . The effect should be well observable in a range of  $x$  and  $Q^2$ , where the acceptance of HERA experiments is well under control.

For given  $x$ ,  $Q^2$ ,  $x_{jet}$  and  $\bar{k}_\perp^2$  the polar angle  $\vartheta_{jet}^{lab}$  in the laboratory frame of the extra jet can be computed, assuming azimuthal symmetry of the cross section in frame where  $\gamma^*$  and the incident proton are collinear [25];  $\vartheta_{jet}^{lab}$  is measured w.r.t. the incoming proton direction. The regions of constant angle  $\vartheta_{jet}^{lab}$  in the  $x_{jet} - \bar{k}_\perp^2$  plane are narrow bands, which are shown as lines for  $Q^2 = 10 \text{ GeV}^2/c^2$ ,  $x = 2 \cdot 10^{-4}$  and  $Q^2 = 100 \text{ GeV}^2/c^2$ ,  $x = 10^{-3}$  (fig. 3.3).

For high values of  $x_{jet}/x$  and small  $\Delta \bar{k}_\perp^2$  the angle is very small. Since particles are lost through the beampipe hole of the detector, jet measurements for  $\vartheta_{jet}^{lab} < 5^\circ$  are not practicable. Moreover, the extra jet has to be identified in close neighbourhood of the target jet, which at small  $x$  is very energetic and has tails in its transverse momentum distribution. Hence there is a sizeable background of particles which lowers

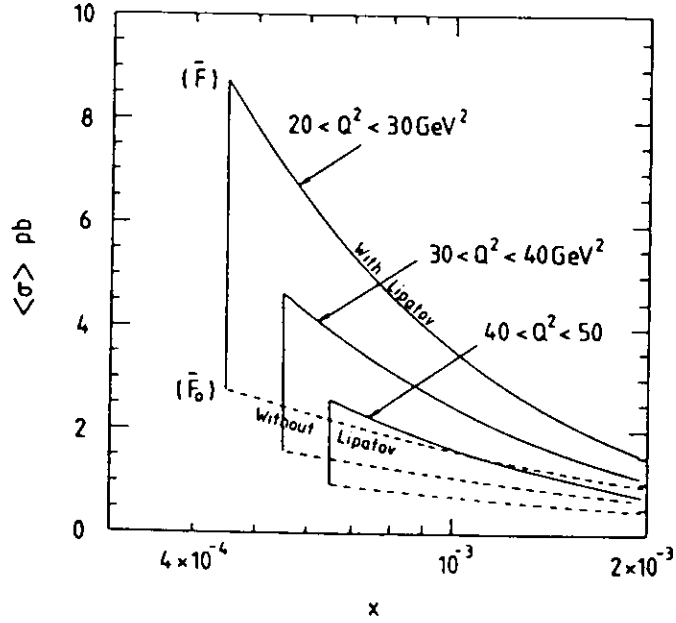


Fig. 3.2. Calculated cross section for DIS + jet ( $\sigma$ ) with  $x_{jet} > 0.05$ ,  $\frac{1}{2}Q^2 < \bar{k}_1^2 < Q^2$ ,  $\vartheta_{jet}^{iab} > 5^\circ$  as a function of  $x$  for bins in  $Q^2$  [24]. The full line shows  $\sigma$  with full gluon radiation ( $\bar{F}$ ), the broken line  $\sigma$  with the gluon radiation ladder suppressed ( $\bar{F}_0$ ).

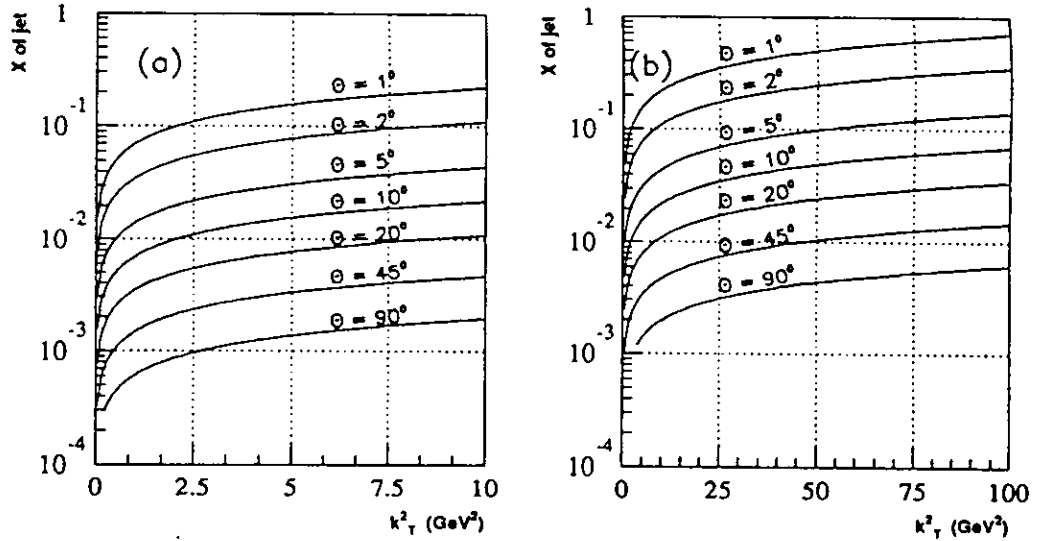


Fig. 3.3. Lines of constant polar angle in the HERA laboratory frame of the extra jet (hot spot search) in the  $x_{jet}$ - $k_T^2$  plane for  $x = 2 \cdot 10^{-4}$ ,  $Q^2 = 10 \text{ GeV}^2/c^2$  (a) and  $x = 10^{-3}$ ,  $Q^2 = 100 \text{ GeV}^2/c^2$  (b) [25].  $k_T^2$  is denoted in the text by  $\bar{k}_1^2$ .

the efficiency of the jet finding algorithm. The correction for the inefficiency is difficult, since an adequate simulation of the target jet properties is needed. The properties of the target jet are not very well known at such low  $x$  values and high values of the hadronic total energy  $W$ .

In  $e-p$  scattering jets may originate from partons produced from the initial state (ISR) or from the final state parton branching (FSR) processes. The jets we are interested in for the hot spot search, come from ISR and have to be separated from the other jet class. This separation seems to be rather problematic since the prediction of pseudorapidity ( $\eta$ ) distributions of partons (jets) in the HERA laboratory frame depend on the details of the implementation of the shower model. This is shown in fig. 3.4 for two different parton shower models. A better understanding of the QCD processes, in particular of the influence of the spacelike shower (ISR) and the interference between ISR and FSR, is necessary. It is the goal of ongoing analyses of the hadronic final state in DIS to shed light on these open questions [26, 27, 28]

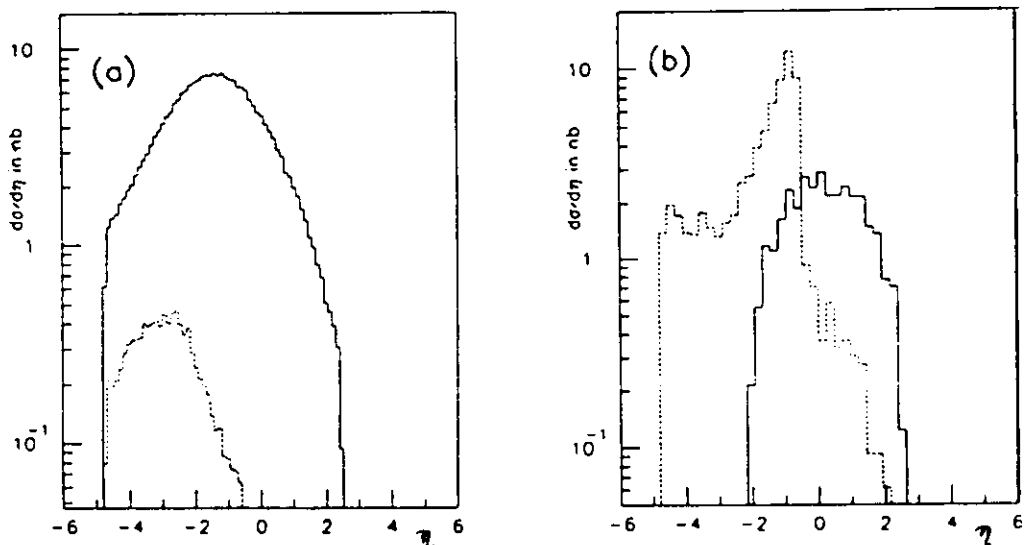


Fig. 3.4. Pseudorapidity distributions in the HERA laboratory frame of final state radiation partons (full line) and initial state radiation partons (dashed line) for events with  $4 \cdot 10^{-4} < x < 10^{-2}$  and  $10 < Q^2 < 100 \text{ GeV}^2/c^2$  [25] (here  $\eta = \ln(\tan \vartheta/2)$ ). Results from two different parton shower simulation programs: (a) LEPTO [29] (b) HERWIG [30].

The application of the technique of TSF measurement makes it possible to study the very interesting new phenomena in parton interaction. However, the analysis has to be supplemented by thorough studies of the hadronic final state in DIS.

## 4 Diffractive Events in Deep Inelastic Scattering

### 4.1 Events with a Large Rapidity Gap

Recently the observation of events in  $e$ - $p$  collision at HERA, in which the hadron closest to the proton beam direction is at a large angle  $\vartheta$ , has been reported [31, 32] (see fig. 4.1). (In the laboratory frame  $\vartheta$  is measured w.r.t. the  $z$  axis along the direction of the incoming proton.) We denote the value of pseudorapidity  $\eta = -\ln(\tan \vartheta/2)$  of the calorimeter cluster with an energy  $E_{cluster} > 0.4$  GeV which is closest to the beampipe hole (the largest observable pseudorapidity is  $\eta = 4.3$  for the ZEUS detector) by  $\eta_{max}$ .

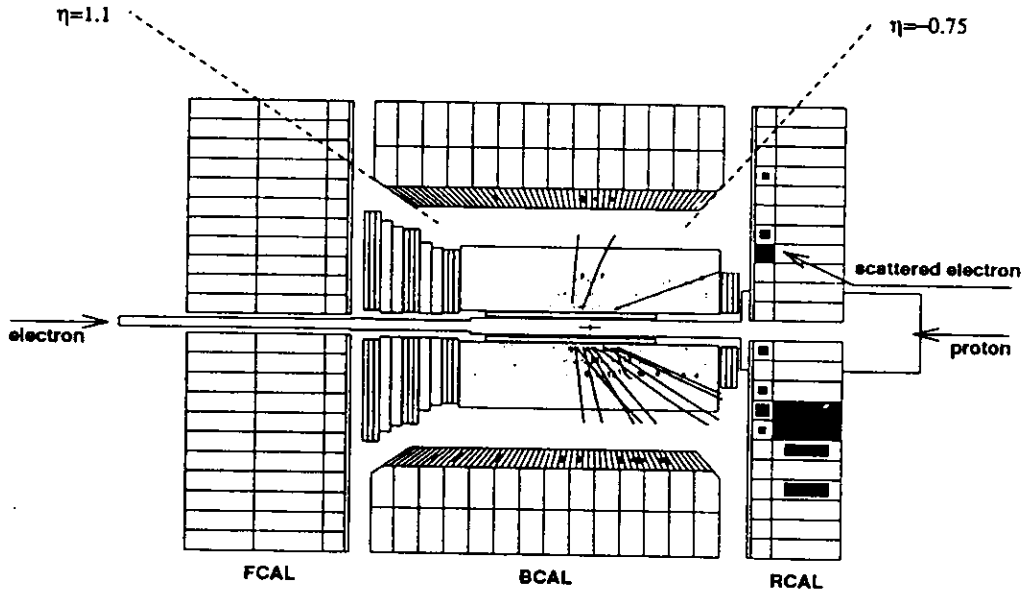


Fig. 4.1. Schematic view of the ZEUS calorimeter and central tracking overlaid by an DIS event with a large rapidity gap. The scattered electron is detected in the rear direction (RCAL).

The events with  $\eta_{max} < 1.5$  are called "large rapidity gap" (LRG) events. The excess of such events seen in the data is not reproduced by models for DIS which are inspired by standard QCD. In fig. 4.3  $M_x^2$ , the invariant mass of the hadronic system observed in the detector, is plotted versus the invariant mass of the  $\gamma^*$ - $p$  system,  $W^2 = (P_{prot} + q_{\gamma^*})^2 = Q^2/x - Q^2$  for LRG events (full points) and the residual DIS events ( $\eta_{max} > 1.5$ ) (see fig. 4.2 for an illustration of the variables). At high  $W^2$  one observes a clear separation of these two event classes. The LRG events are distinguished by a large ratio  $W^2/M_x^2$ . The  $M_x^2$  distribution is steeply falling, as one expects for diffractive like events, whereas the event distributions in  $W^2$  and  $Q^2$  resemble those of standard DIS events.

The characteristics of LRG events found so far, are suggestive of a diffractive interaction between a highly virtual photon and the proton, which is mediated by the exchange of a pomeron. From fig. 4.3 it becomes plausible, why this type of events

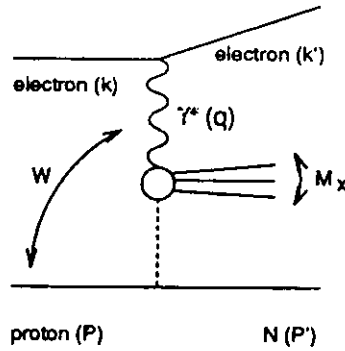


Fig. 4.2. Schematic diagram describing particle production by diffractive dissociation DIS events.

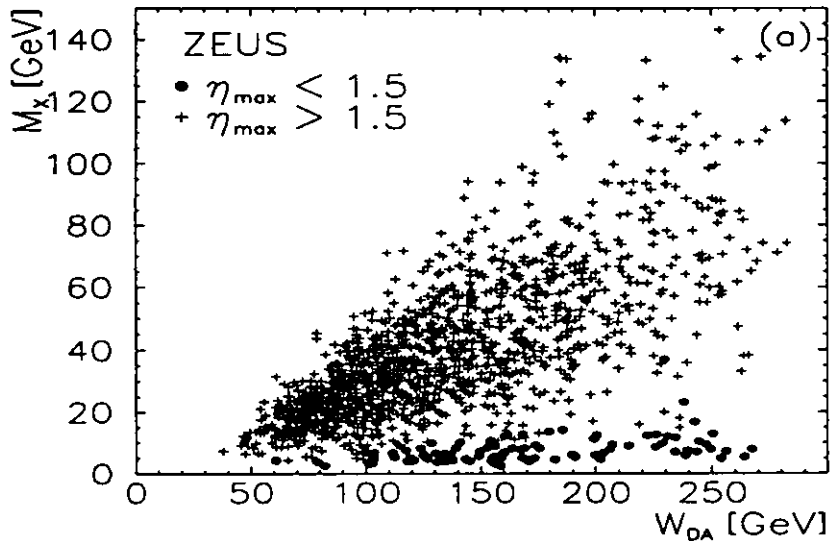


Fig. 4.3. Correlation between the invariant mass  $M_x$  of the hadrons observed and the invariant mass  $W_{DA}$  of the  $\gamma^*p$  system. The index "DA" denotes the method of the reconstruction of the variable  $W$  [31].

could not have been observed in previous DIS experiments. The center of mass energy was too low so that the range of  $W$ , where the event classes are separable, could not be reached.

#### 4.2 Diffractive Events in $p\bar{p}$ Collisions and the Pomeron

The more direct way to tag a diffractive process is by measuring the diffractively scattered proton in a suitable detector for leading protons in the very forward direction. In the UA8 experiment at the SPS/CERN diffractive  $p\bar{p}$  reactions with associated jet production ( $p\bar{p} \rightarrow p_{diff} + jet(s) + X$ ) have been searched for. Conventional diffractive

processes are dominated by the exchange of a pomeron Regge trajectory. It was pointed out [33], that by demanding jet production, hard diffractive reactions are selected, so that the partonic structure of the pomeron could be investigated.

In fact a clean 2-jet structure with little underlying event background has been observed in events with a fast proton ( $x_P = P'/P_{inc} > 0.9$ ) measured in the leading proton detector [34]. Such events can be interpreted as an interaction of the  $\bar{p}$  with a pomeron dominated component of the proton, which carries a small fraction of the proton momentum  $x_{pom} = (1 - x_P) \ll 1$ . The hard scattering from which the two jets emerge, takes place between a parton from the  $\bar{p}$  and one from the pomeron. The spectator jets of the  $\bar{p}$  and the pomeron are expected to dissappear in the beampipe holes.

In analogy to the  $x_F$  variable in the  $\gamma^*p$  cms of the DIS process, scaling variables  $x_{1jet}$  ( $x_{2jet}$ ) can be defined in the pomeron- $\bar{p}$  cms:  $x_{1jet} = 2\tilde{k}_{1j}^{\parallel}/\sqrt{s'}$  and  $x_{2jet} = 2(\tilde{k}_1^{\parallel} + \tilde{k}_2^{\parallel})/\sqrt{s'}$  where  $s' = s(1 - x_p)$  is the invariant mass of the  $\bar{p}$ -pomeron system.  $\tilde{k}_i^{\parallel}$  is the momentum component parallel to the  $\bar{p}$  measured in the  $\bar{p}$ -pomeron cms. Neglecting the effect of gluon radiation, at the parton level  $x_{2jet}$  measures the difference between the scaled fractional momenta of the incident partons which participate in the hard interaction:  $x_{2jet} = x_{pom} - x_{\bar{p}}$  with  $x_{pom} = p_{parton/pom}/P_{pom}$  and  $x_{\bar{p}}$  defined analogously.

In fig. 4.4 (from [33]) the measured  $x_{2jet}$ -distribution for 2-jet events is compared with the result of a model calculation using a factorization ansatz for the cross section with two pomeron structure functions ( $F_2^{pom}$ ) which represent two extreme hypotheses. The MC data have been processed through the detector simulation and event reconstruction program. A hard pomeron structure function is favoured by the experimental results. It is argued that the excess of data over MC events around  $x_{2jet} \sim 0.6$  can be explained by an admixture of a "superhard" ( $\delta(x_{pom} - 1)$ ) component in  $F_{2,pom}$ , which is smeared out due to the effects of the hadronization and the detector resolution (see fig. 4.4b). It is tempting to use this information directly for model calculations in DIS. But considering the possibility of a coherent diffractive component one might have to call into question the validity of the factorization hypothesis [35].

### 4.3 Pomeron in Deep Inelastic $e-p$ Collisions

It has always been argued that at sufficiently small  $x$  the DIS cross section becomes like the real photoproduction cross section ("Regge limit"). This assumption has been used when extrapolating  $F_2$  to  $x \rightarrow 0$  e.g. for the evaluation of sum rules from measured data [36, 37, 38, 39]. The first direct signal for the hadronic nature of a virtual photon came from deep inelastic  $e-A$  scattering. The nuclear shadowing at small  $x$  ( $x < \sim 0.05$ ) can be explained in a consistent way if a significant hadronic component in the virtual photon is assumed ( see sect. 2.1).

The existence of a diffractive component in DIS, as predicted many years ago [41], is well in line with this picture. A wealth of data from total cross sections and cross sections for diffractive scattering in hadron hadron interactions are successfully described within the pomeron exchange picture [40]. The pomeron was introduced as

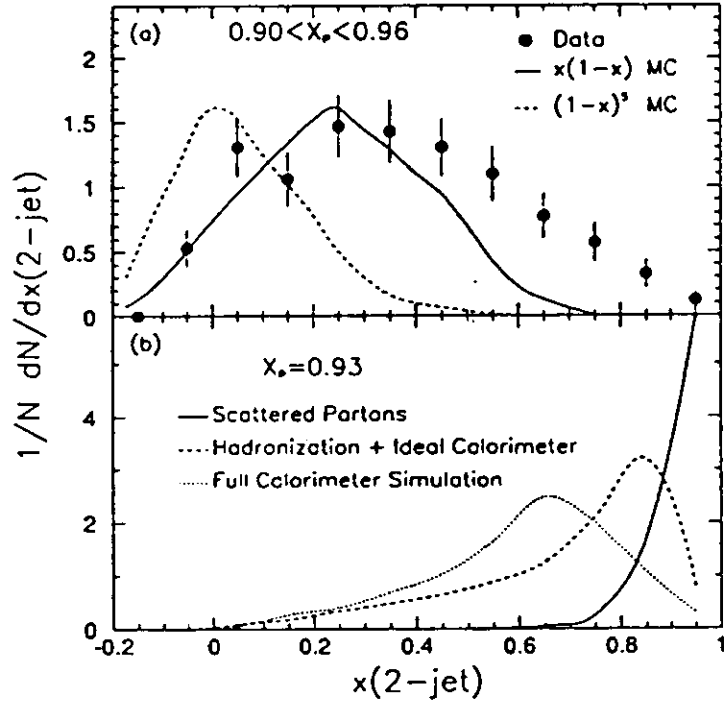


Fig. 4.4. Observed  $x_{2jet}$  distribution for  $p\bar{p}$  events with a leading proton ( $x_p > 0.9$ ) and 2 jets in the main detector. (a) Comparison of the data with MC calculation using a hard (full line) and a soft (dashed line) structure function for the pomeron (arbitrary normalisation). (b) Result of a  $x_{2jet}$  spectrum if the pomeron structure function is  $\delta(1 - x_{pom})$  after hadronization and detector smearing.

the mediator of the exchange forces in reactions where only energy and momentum but no quantum numbers are transferred. Formally one can ascribe a Regge trajectory to the pomeron in the same way as for a real particle, but the question about its nature is not answered at all.

Many models suggesting an internal structure of the pomeron have been developed since the first publication of results on hard diffractive  $p\bar{p}$  scattering from UA8 [42].

Based on experimental data from soft hadron hadron interactions (e.g. additive quark rule for  $\sigma_{tot}^{hh}$ ) it is argued that the pomeron has a quark-antiquark structure [41, 43]. The suggestion that the pomeron is mainly composed of gluons is rather old [44] and revived in more recent analyses [45, 46] and in the context of the results from the UA8 experiment. The latter idea relies on the factorization hypothesis, i.e. that the pomeron is considered as a quasi-particle in the proton so that the diffractive structure function  $F_2^{diff}$ , which is defined in analogy to the  $F_2$  in DIS, can be factorized by:

$$f_{pom/P}(x_{pom}, t) * F_2^{pom}\left(\frac{x}{x_{pom}}, Q^2\right) \quad (4.1)$$

namely into the pomeron flux in the proton and the pomeron structure function, for which several functional ansatzes are discussed (see sect. 4.2).

Nikolalev and Zakharov describe diffractive dissociation (DD) of the photon by the exchange of two non interacting gluons as shown schematically in fig. 4.5 [49]. The pair of gluons is colourless as seen from outside. They define an effective  $F_2^{pom}$  by:  $F_2^{pom}(x_{pom}, Q^2) = \frac{Q^2}{4\pi^2\alpha^2} \sigma_{\gamma-pom}(M_x^2)$  introducing  $\sigma_{\gamma-pom}$ , the photon pomeron in-

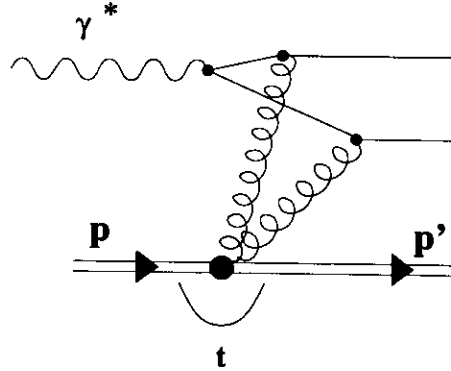


Fig. 4.5. Schematic diagram of the model for diffractive dissociation discussed in [49].

teraction cross section. ( $x_{pom} = Q^2/(Q^2 + M_x^2)$  is the the Bjorken- $x$  variable for the pomeron).  $F_2^{pom}$  has a hard component ( $\propto x_{pom}(1 - x_{pom})^2$ ) and a softer contribution from the triple pomeron coupling [48]. The concept of a pomeron structure function, expressed in terms of gluon ladders ( see sect.3.1) leads to a soft structure function for the part which could be treated by perturbative QCD.

Diffractive dissociation in DIS is a suitable process to obtain information about the internal structure of the pomeron. In numerous publications (e.g. [33, 41, 47, 49, 48]) this process is considered the most direct and cleanest method to determine the pomeron structure. The high center of mass energy available make the study of DD at HERA particularly attractive.

#### 4.4 Towards the Analysis of the Pomeron Structure ?

Deep inelastic  $e-p$  collisions with a large rapidity gap and characteristics of diffractive dissociation (DD) of virtual photons, have already been observed at HERA. In these measurements the forward going proton of low mass nuclear system was not yet detected. Recently, ZEUS has, however, commissioned a leading proton spectrometer (LPS) downstream of the interaction region along the proton beam, where the longitudinal and transverse momentum of a leading proton can be measured.

The LPS consists of 6 measurement stations (Roman Pots) equipped with silicon microstrip detectors positioned before and after bending magnets [50]. Only the three most downstream stations have been read out so far. Fig. 4.6 shows an event picture from the ZEUS detector, where a deep inelastic scattering has occurred and at the same time a track in the LPS has been recorded. The silicon microstrips which are hit are

displayed on the left hand side of the figure. The scattered electron is seen in the rear part of the main calorimeter ( right hand side of the figure) and the associated hadron jet(s) in the barrel and forward calorimeter.

Leading Proton Spectrometer

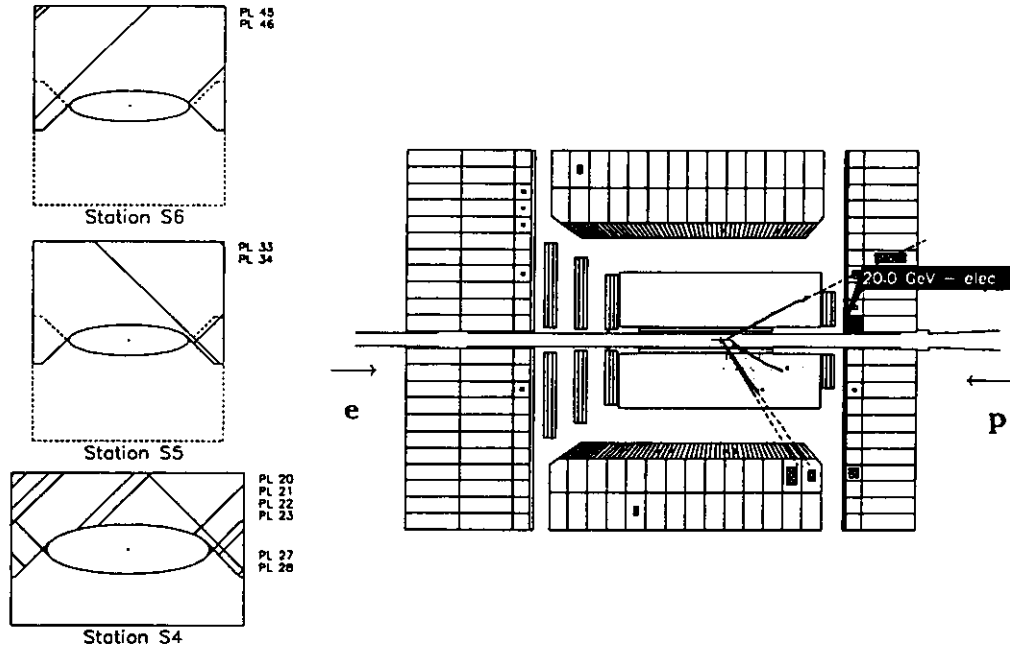


Fig. 4.6. Schematic diagram of the ZEUS main calorimeter and central tracking. A DIS event with a large rapidity gap is shown, for which a track in the detector planes of the leading proton has been recorded (left part of the figure). The kinematic variables reconstructed for this event are:  $x = 0.7 \cdot 10^{-3}$ ,  $Q^2 = 13 \text{ GeV}^2/c^2$ .

With the LPS it will be possible to tag DD events without requiring a very large rapidity gap. This is advantageous because the cut on large rapidity gaps biases the event selection towards a sample at high  $W^2$ . As long as one has no reliable physics model to simulate diffractive processes, it is difficult to correct for this effect and to determine absolute cross sections. Furthermore the contribution from standard DIS to the production of large rapidity gap events has to be determined.

With a large sample of well identified DD events one can tackle more ambitious tasks, for example testing a possible component of the pomeron which can be calculated in the framework of perturbative QCD [48, 21]. One has to search for diffractive DIS events, in which the hadron closest to the rapidity gap has a large transverse momentum  $\vec{k}_1^2$  (where  $\vec{k}_1^2$  is measured in a frame in which the momenta of  $\gamma^*$  and incoming proton are collinear). For an illustration see fig. 3.1 with the distinction, that the spectator

jet has to be replaced by the diffractively scattered proton  $p'$  and that no condition for the momentum fraction  $x_{jet}$  has to be applied. In this case the pomeron would also be probed with a high resolution ( $\bar{k}_1^2 \sim Q^2$ ).

## 5 Concluding Remarks

The measurement of tagged structure functions in electron nucleus/nucleon scattering opens up the possibility to investigate very subtle and interesting processes in high energy physics, as demonstrated by the examples discussed in this report. However, the requirements on the detector and analysis methods might be challenging.

Tagged structure function analyses are clearly difficult. This is inherent to the method, since this technique is destined to search for tiny effects in the presence of a large background from the "standard" events. Not only high luminosity and more sophisticated detectors are needed, but also a better understanding of the concurrent processes, so that the background from standard processes can be subtracted or corrected for.

## Acknowledgements

It is a pleasure for me to thank Louk Lapikas, Piet Mulders, Jona Oberski and their colleagues for the excellent organisation of the conference and the warm hospitality in the NIKHEF institute. I am grateful to Piet Mulders for his kind invitation to this conference.

## References

- [1] ZEUS Collaboration, 'The ZEUS Detector', Status Report 1993.
- [2] EMC Collab., J.J. Aubert et al., Phys. Lett. B123 (1983) 123.
- [3] H. Peschel, Ph.D. thesis, Univ. Wuppertal, WUB 90-13.
- [4] B. Badelek, J. Kwieciński, Phys. Lett. B208 (1988) 508.  
A.H. Mueller, J. Qiu, Nucl. Phys. B268 (1986) 427.  
J. Qiu, Nucl. Phys. B291 (1987) 746.  
E.L. Berger, J. Qiu, Phys. Lett. B206 (1988) 141.
- [5] N.N. Nikolaev, V.I. Zakharov, Phys. Lett. B55 (1975) 397.  
N.N. Nikolaev, V.I. Zakharov, Phys. Lett. B260 (1991) 414.  
L. Frankfurt, M. Strikman, Nucl. Phys. B316 (1989) 340.  
S.J. Brodsky, H.J. Lu, Phys. Rev. Lett. 64 (1990) 1342.
- [6] L. Frankfurt, M. Strikman, Phys. Rep. 160 (1988) 235.
- [7] A. Bodek, J.L. Ritchie, Phys. Rev. D23 (1981) 1070.  
E.L. Berger, F. Coester, R.B. Wiringa, Phys. Rev. D29 (1984) 398. R.P. Bickerstaff, Proc. Int. Conf. on "Medium and High Energy Nuclear Physics", Taipei/Taiwan (1988), p 99.

- [8] L.C. Bland, contribution to Proc. of this Conference.  
L.H. Keester, contribution to Proc. of this Conference.  
T. Hehl, contribution to Proc. of this Conference.  
T. Wagner, contribution to Proc. of this Conference.  
H.P. Blok, contribution to Proc. of this Conference.
- [9] M. Radici, contribution to Proc. of this Conference.  
C. Guisti, F.D. Pucati, Nucl. Phys. A535 (1991) 537.
- [10] C. Ciofi degli Atti, S. Simula, Proc. of Workshop on "European Electron Facility", Mainz (1992), p. 423.
- [11] C.H. Llewellyn-Smith, Phys. Lett. B128 (1983) 107.  
B.L. Friman et al., Phys. Rev. Lett. 51 (1983) 763.  
M. Ericson, A.W. Thomas, Phys. Lett. B148 (1984) 191.  
B.L. Bibair, E.M. Levin, A.G. Shuvaev, Nucl. Phys. A491 (1989) 618.  
W.Z. Ben, Z. Phys. C46 (1990) 293.
- [12] R.P. Bickerstaff, A.W. Thomas, J. Phys. G15 (1989) 1523.
- [13] G.L. Li et al., Phys. Lett. B213 (1988) 531.
- [14] S.V. Akulinichev et al., Phys. Rev. Lett. 55 (1985) 2239.
- [15] C. Ciofi degli Atti, Simula, preprint INFN-ISS 93/94 (June 1993)
- [16] O. Bing et al., Proc. of the Workshop on "European Electron Facility", Mainz (1992), p. 475
- [17] L.L. Frankfurt, M.I. Strikman, Physics Reports 160 (1988) 235.
- [18] G.D. Bosveld, A.E. Dieperink, O. Scholten, Phys. Rev D26 (1982) 1061.
- [19] Proc. of the Workshop on "European Electron Facility", Mainz (1992).
- [20] see e.g. review by  
M. Virchaux, Proc. of the Workshop "QCD - 20 Years Later", Aachen (1992), p 205.
- [21] L.V. Gribov, E.M. Levin, M.G. Ryskin, Phys. Rep. 100 (1983) 1.
- [22] A.H. Mueller, H. Navelet, Nucl. Phys. B282 (1987) 727.  
A.H. Mueller, Nucl. Phys. B18C (Proc. Suppl.) (1991) 125.
- [23] J. Bartels, M. Loewe, A. de Roeck, Z. Phys. C54 (1992) 635.
- [24] J. Kwieciński, A.D. Martin, P.J. Sutton, Phys. Lett. B287 (1992) 254.
- [25] J. Bartels et al., Proc. of the Workshop on "Physics at HERA", Hamburg (1992), p 203.
- [26] H1 Coll., T. Ahmed et al., Phys. Lett. B298 (1993) 469.
- [27] ZEUS Coll., M. Derrick et al., Z. Phys. C59 (1993) 231.
- [28] O. Deppe, T. Haas, N.A. Pavel, Zeus int. report 93-106 (1993).
- [29] G. Ingelmann, Workshop on "Physics at HERA", Hamburg (1992), p 1366 and ref. therein.

- [30] B. Webber, Workshop on "Physics at HERA", Hamburg (1992), p 1354 and ref. therein.
- [31] ZEUS Coll., M. Derrick et al., Phys. Lett. B315 (1993) 481.
- [32] H1 Coll., B. Andrieu et al., DESY 93-146 (1993).
- [33] G. Ingelmann, P. Schlein, Phys. Lett. B152 (1985) 256.
- [34] A. Brandt et al., Phys. Lett. B297 (1992) 417.
- [35] J. Collins, L.L. Frankfurt, M.I. Strikman, Phys. Lett. B307 (1993) 161.
- [36] EMC Coll., J. Ashman et al., Nucl. Phys. B328 (1989) 1.
- [37] SMC Coll., B. Adeva et al., Phys. Lett. 302 (1993) 533.
- [38] E142 Coll., P.L. Anthony et al., "Determination of Neutron Spin Structure Function", SLAC-PUB-6101 (1993).
- [39] NMC Coll., P. Amaudruz et al., Phys. Rev. Lett. 66 (1991) 2712.
- [40] A. Donnachie, P.V. Landshoff, Nucl. Phys. B244 (1984) 322.  
A. Donnachie, P.V. Landshoff, Nucl. Phys. B267 (1985) 690.
- [41] A. Donnachie, P.V. Landshoff, Phys. Lett. B191 (1987) 309.
- [42] UA8 Collab., R. Bonino et al., Phys. Lett. B211 (1988) 239.
- [43] A. Donnachie, P.V. Landshoff, Nucl. Phys. B303 (1988) 634.
- [44] F.E. Low, Phys. Rev. D12 (1975) 163.  
S. Nussinow, Phys. Rev. Lett. 34 (1975) 1286.
- [45] E.L. Berger et al., Nucl. Phys. B286 (1987) 704.
- [46] G. Ingelmann, K. Prytz, Z. Phys. C58 (1993) 285.
- [47] K.H. Streng, Proc. of the HERA Workshop, Hamburg (1987) p 367.
- [48] J. Bartels, G. Ingelmann, Phys. Lett. B235 (1990) 175
- [49] N.N. Nikolaev, B.G. Zakharov, Z. Phys. C53 (1992) 331
- [50] ZEUS Collaboration, 'The ZEUS Detector', Status Report 1993.

3

2

1

2